ASIAN JOURNAL OF CIVIL ENGINEERING (BHRC) VOL. 14, NO. 4 (2013)
PAGES 557-576

NUMERICAL MODELING OF REINFORCED CONCRETE COLUMNS STRENGTHENED WITH COMPOSITE MATERIALS

M.A. Barkhordari[*a], N. Dayhim[a] , A. Nicknam[a] , M. Razi[a] and S. Mehdizad[b]
[a] Department of Civil Engineering, Iran University of Science and Technology, Tehran, Iran
[b] Department of Civil Engineering, Sharif University of Technology, Tehran, Iran

Received: 5 August 2012; **Accepted:** 15 January 2013

ABSTRACT

The use of Near-surface Mounted (NSM) FRP bars is an efficient strengthening technique to enhance the flexural strength of RC structures. This article is intended to analytically investigate the effectiveness of Glass Fiber Reinforced Polymer (GFRP) bars in combination with GFRP wraps on the flexural capacity of reinforced concrete (RC) columns with Fiber Element Modeling approach. The accuracy and reliability of the proposed fiber-based modeling method is demonstrated by numerical models on seven half-scale experimental RC reference columns under axial and cyclic lateral loads. These reference specimens are comprised of seven half-scale RC columns including two unstrengthened and five strengthened specimens with two GFRP bar reinforcement ratios under three axial load levels. Additionally, eight RC strengthened columns are analytically simulated with four complementary GFRP bar reinforcement ratios under two axial load levels. As the numerical results represent good correlation between the fiber-based modeling approach and the experimental results of the reference RC columns, it is concluded that the numerical simulations explicitly predict a considerable improvement in the flexural strength of the RC columns retrofitted with Glass Fiber Reinforced Polymer bars.

Keywords: GFRP bar; near-surface mounted (NSM); GFRP wrap; flexural strengthening; fiber element model (FEM).

1. INTRODUCTION

Two different modeling philosophies are widely used in analytically reproducing the inelastic response of structures under seismic action. These modeling philosophies are comprised of the ‘concentrated plasticity’ and the ‘distributed inelasticity’ modeling approaches.

[*] E-mail address of the corresponding author: barkhordar@iust.ac.ir (M. A. Barkhordari)

The ‘concentrated plasticity’ approach is concerned with a frame element consists of two zero-length nonlinear rotational spring elements connected by an elastic element [1-3]. The nonlinear behavior of a structure is attained by the nonlinear moment–rotation relationships of these spring elements. Among the proposed concentrated plasticity constitutive models, a number of them include stiffness degradation in flexure and shear [4-6], several include pinching under reversed cyclic loading [6,7], and numerous models comprise fixed-end rotations at the beam-column joint interface to simulate the effect of bar pull out [8,9]. In this lumped plasticity approach, the accuracy of the analysis may be compromised whenever users are not highly experienced while calibrating the available response curves required to describe the concentrated plasticity elements. The limitations of concentrated plasticity models are discussed in numerous studies [10,11].

The ‘distributed inelasticity’ model more accurately illustrates the continuous structural characteristics of Reinforced Concrete (RC) members. This nonlinear modeling approach requires simply geometrical and material characteristics as input data.

In the distributed inelasticity modeling approach, the constitutive behavior of the cross-section of RC members either can be formulated using the classical plasticity theory in the form of stress-strain resultants, or concluded by discretizing the cross-section into fibers, known as “Fiber Element Modeling” (FEM) as shown in Figure 1.

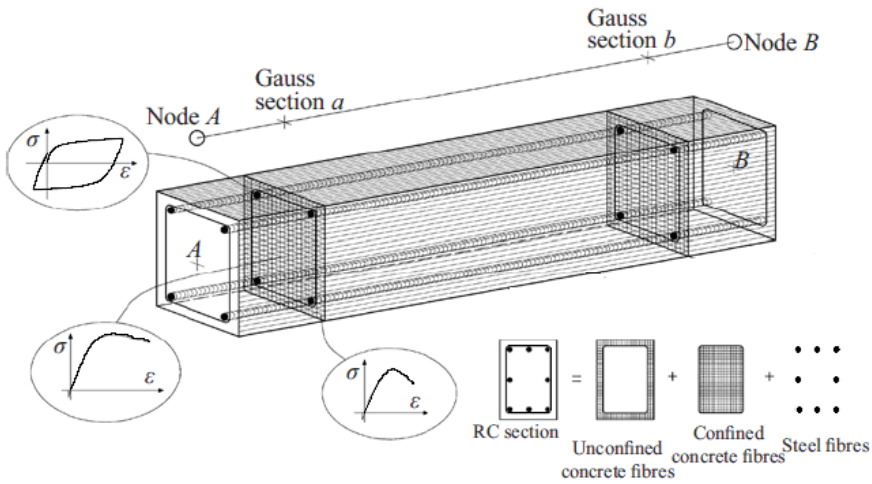

Figure 1. Fiber beam-column element in the local reference system, discretization of a typical concrete cross-section into fibers

In the initial phases concerning the application of the distributed nonlinearity modeling approach, these elements were formulated using the classical stiffness approach with cubic hermitian polynomials to estimate the deformations along the element [12,13]. Menegotto and Pinto [14] interpolated section deformations along with section flexibilities and considered the axial force-bending moment interaction. Shear effects were first employed in the model proposed by Bazant and Bhat [15]. Additionally, alternative flexibility-based formulations have been developed by Mahasuverachai and Powell, Kaba and Mahin, Zeris and Mahin [16-19]. These formulations caused difficulties during their implementation in fiber-based modeling programs. To overcome such complexities, Ciampi and carlesimo [20]

suggested a reliable flexibility-based approach in order to formulate frame member models. In addition, this flexibility-based approach was employed by Spacone [21] to formulate the beam-column element in FE modeling. A number of researchers such as Papaioannoa et al. [22] have shown a detailed discussion on the differences among stiffness-based and flexibility-based approaches.

Fiber Reinforced Polymer (FRP) composite jacketing system is an efficient technology for upgrading the shear strength, flexural ductility and axial resistance of RC columns. Over the last decade, a number of researchers have demonstrated the effectiveness of FRP composites in improving the seismic performance and capacity of structures [23-26]. FRP jacketing system provides lateral confinement which ends up with an increase in the concrete compressive strength as well as the ultimate strain of concrete [23-25]. This confinement effect prevents the buckling of the longitudinal steel bars, restrains the lateral concrete expansion and causes delay in the spalling of cover concrete.

Traditionally, the flexural capacity of RC members is modified by FRP sheets [24-26]. In this method, the vertical FRP sheets parallel to the longitudinal steel reinforcements, anchored by steel anchorages, is used to increase the flexural capacity of RC columns. In this technique, FRP sheets should be anchored to the adjacent members. Such anchorages may cause the premature rupture of FRP sheets due to the stress concentration in anchorage zone [26].

The use of Near-surface Mounted (NSM) FRP bars is an alternative strengthening technique to upgrade the flexural strength of RC structures [27-33]. The advantages of NSM-FRP bars in comparison with externally bonded FRP composites to improve the flexural capacity of RC beams have been successfully shown by De Lorenzis and Nanni, El-Hacha and Rizkalla, Parretti and Nanni and Yost et al. [29-33]. An important advantage of NSM-FRP bars with respect to externally bonded FRP composites is the possibility of anchoring reinforcements into adjacent members, as shown by Nanni et al. [34]. This technique becomes particularly attractive for the flexural strengthening in the negative moment regions of slabs and girders, where externally bonded FRP composites can be subjected to severe damages due to the mechanical and environmental conditions [34]. This technique does not need any surface preparation work and can be accomplished with minimal installation time after cutting the grooves as compared with externally bonded FRP composites, because the use of primer and putty is normally not necessary [35].

Recently, Bournas and Triantafillou [36] have experimentally demonstrated that the flexural resistance and ductility of RC columns under seismic loading can be enhanced by NSM-FRP bars in combination with CFRP wraps. In full scale tests carried out by Alkhrdaji et al. [35], it was concluded that using Glass Fiber Reinforced Polymer (GFRP) bars with higher strain and lower modulus compared to Carbon Fiber Reinforced Polymer (CFRP) bars, leads to higher structural ductility in the flexural strengthening of RC columns.

Additional to the above mentioned studies, still more experimental and analytical research work is needed to evaluate the upgrading levels of the flexural capacity of RC columns by longitudinal GFRP bars. This idea has been the main motivation of this study. This article is intended to simulate the specimens with fiber-based modeling approach in order to analytically investigate the flexural strength of RC columns reinforced by longitudinal NSM-GFRP bars along with GFRP wraps under axial and cyclic lateral loads.

2. FIBER ELEMENT MODELING, MATERIAL PROPERTIES AND CONSTITUTIVE MODELS

2.1 Overview of the Experimental Reference Specimens

The experimental reference specimens were square RC columns, consisted of 250 mm wide and 900 mm long, connected to a 300 mm×400 mm×850 mm stub. These specimens were comprised of six longitudinal steel bars with diameter of 12 mm (ρ_l =1.08 %, where ρ_l is the ratio of longitudinal steel reinforcement area to gross area of concrete) and were confined with transverse steel ties with diameter of 8 mm spaced at 100 mm (ρ_s =1.4 %, where ρ_s is the volumetric ratio of transverse steel ties to core concrete). The details of the experimental reference specimens and test set-up are shown in Figure 2.

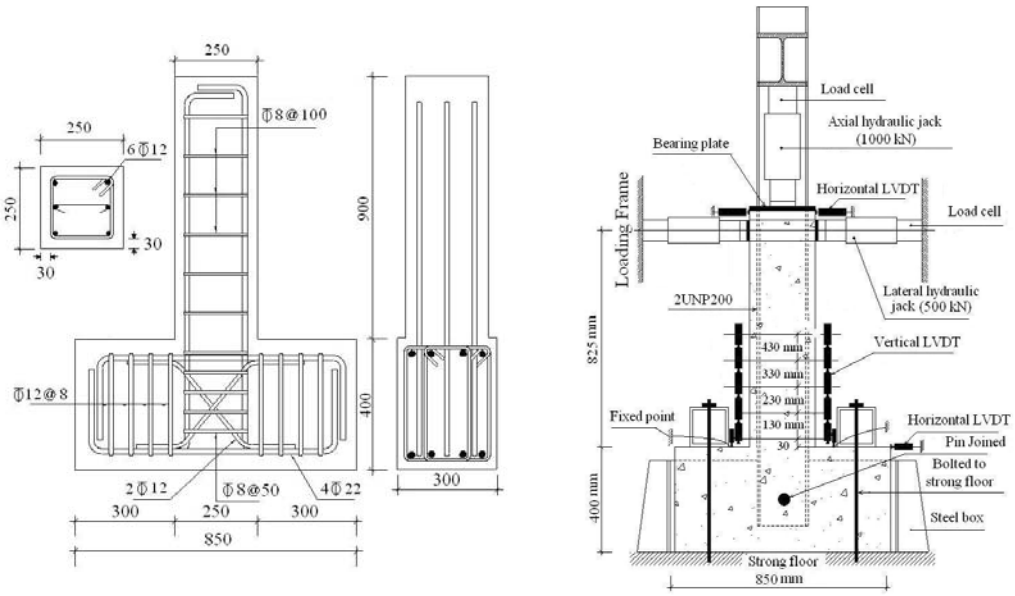

a) b)

Figure 2. a) Details of the experimental reference specimens (all dimensions are in mm); b) Test set-up and location of instrumentations

2.2 Fiber Element Model

The Fiber Element Model (FEM) represents the spread of material inelasticity along the member length and across the cross-section area of RC members. By discretizing the cross-section into fibers, realistic modeling of different materials is possible; thereby, an accurate estimation of the structural damage distribution is concluded up to a highly inelastic deformation range. A number of fiber-based modeling programs are available for nonlinear analysis of RC structures in the literature [37-39]. The authors utilized SeismoStruct [39], which is a fiber-based modeling program in order to seismic analysis of framed structures. This fiber element modeling software can be downloaded at no charge from the internet and also is simple to employ, even for inexperienced users.

The simulated and experimental reference specimens have been given descriptive names. Each column is identified with an acronym, where C denotes control for the unstrengthened experimental reference specimens, R indicates retrofitted for the strengthened experimental reference specimens and P indicates predicted for the simulated specimens.

Seven half-scale RC reference specimens consisted of two unstrengthened specimens C_1 and C_2 and five strengthened specimens R_1 to R_5 were experimentally and analytically investigated to study the influence of NSM-GFRP bars on their flexural capacity. The specimens R_2 to R_5 were strengthened with two different GFRP bar reinforcement ratios, (ρ_{NSM} =0.5% and 0.75%, where, ρ_{NSM} , is the ratio of longitudinal GFRP reinforcement area to gross area of concrete), and were tested under three axial load levels ($P = 0$, $P = 0.1 f_c' A_g$ and $P = 0.2 f_c' A_g$) and cyclic lateral loads. Figure 3 shows the details of the unstrengthened and strengthened experimental reference specimens. With the aim of verifying the validation of numerically reproducing reference specimens by fiber element modeling approach, a comparison was accomplished between the experimental results and fiber-based modeling analyses of seven half-scale reference specimens.

Furthermore, eight additional RC strengthened specimens P_1 to P_8 were analytically simulated using Fiber Element Modeling approach with four supplementary GFRP bar reinforcement ratios (ρ_{NSM} = 0.1%, 0.2%, 0.3% and 0.4%) under two axial load levels, (P =0 and P =0.2 $f_c' A_g$) and cyclic lateral loading. Table 1 shows the details of the simulated and experimental reference specimens.

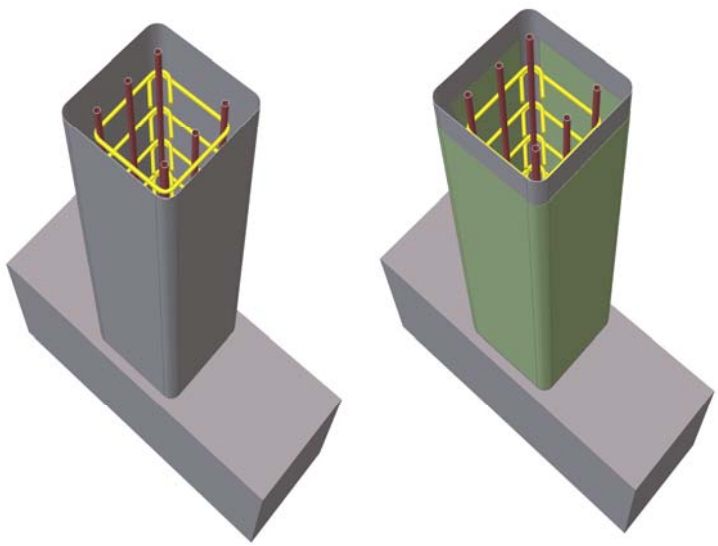

a) b)

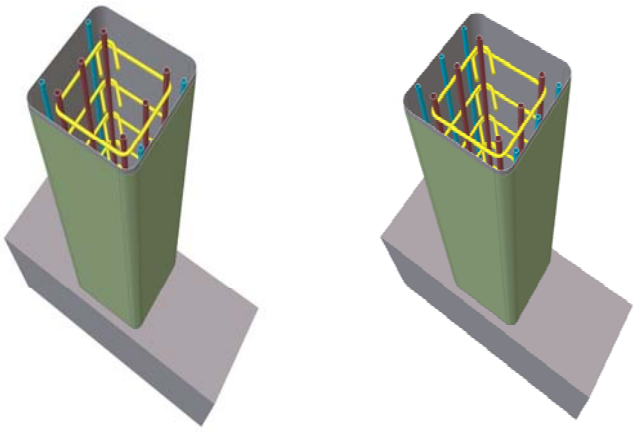

c) d)

Figure 3. Details of the experimental reference specimens: a) unstrengthened specimens C_1 and C_2; b) strengthened specimen R_1 (3 layers of GFRP sheets); c) strengthened specimens R_2, R_3 and R_4 (4 NSM GFRP bars + three layers of GFRP sheets); d) strengthened specimen R_5 (6 NSM GFRP bars + three layers of GFRP sheets)

The effect of earthquake was modeled by applying reversed cyclic lateral loading, including 26 loading-reloading cycles. Figure 4 shows cyclic lateral loading procedure of the specimens.

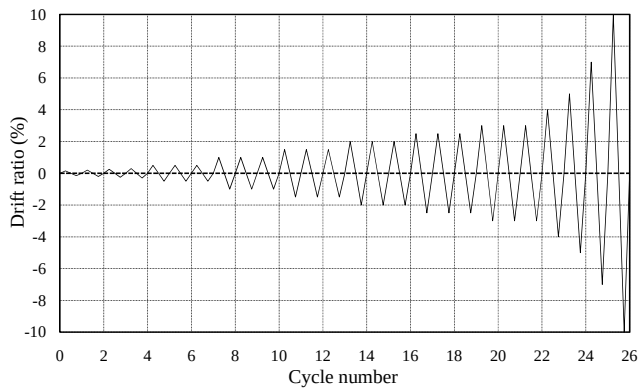

Figure 4. Loading procedure

Table 1: Details of simulated and experimental reference specimens

Specimen	Longitudinal Steel		Transverse steel		f_c' (MPa)	$\frac{P}{f_c' A_g}$	Strengthening regime	
	Diam. (mm)	ρ_l (%)	Diam. (mm)	ρ_s (%)			ρ_{NSM} (%)	No. of layers of GFRP sheets
C_1	12	1.08	8	1.4	34.5	0	na	na

C_2	33.7	0.2	na	na
P_1	35	0	0.1	3
P_2	35	0	0.2	3
P_3	35	0	0.3	3
P_4	35	0	0.4	3
P_5	35	0.2	0.1	3
P_6	35	0.2	0.2	3
P_7	35	0.2	0.3	3
P_8	35	0.2	0.4	3
R_1	32.9	0.2	na	3
R_2	36.1	0	0.5	3
R_3	34.7	0.1	0.5	3
R_4	38.7	0.2	0.5	3
R_5	36.5	0.2	0.75	3

Note: f_c', concrete compressive strength; na, not applicable; ρ_{NSM}, the ratio of longitudinal GFRP reinforcement area to gross area of concrete.

2.3 Material Properties

The reference specimens were designed for target strength of 35 MPa. The strength of each experimental reference specimen (C_1, C_2, and R_1 to R_5) was determined by averaging the values obtained from three standard cylinder tests (see Table 1). The properties of the longitudinal steel bars, GFRP bars, GFRP composite sheets and epoxy system are shown in Table 2. Grade 400 steel was used for longitudinal and transverse steel bars.

Table 2: Mechanical properties of materials

Material	**Diameter (mm)**	**Elastic modulus (GPa)**	**Yield strength (MPa)**	**Tensile strength (MPa)**	**Ultimate strain [a] (%)**
GFRP sheet	0.33	77	-	1694	2.2
Epoxy paste	-	10	-	60	-
GFRP bar	10	43	-	900	2.09
Steel bar	8; 12; 22	210	400	600	15

[a] **Based on tension coupon test.**

2.4 Fiber Constitutive Models

The software utilized herein, SeismoStruct [39], is capable of reproducing large displacement behaviors up to a highly inelastic range and collapse load of framed structures subjected to static or dynamic loading. Geometric nonlinearity and material inelasticity are

accounted for while utilizing this software. The nonlinear behavior of an element by means of the fiber-based modeling approach is derived from the nonlinear behavior of the fibers in the considered cross-section. Consequently, the validity of the analytical results in fiber modeling approach depends on the accuracy of the fiber material models. These fiber material models may feature different levels of accuracy or complexity in their definition in the numerical analyses. In fiber-based modeling approach, a cross-section of RC column is subdivided, distinguishing steel, composite, confined and unconfined concrete (Figure 5). For GFRP composite materials, the stress-strain relationships are completely linear up to the failure. In fiber-based modeling approach, the sectional stress-strain state of the elements is attained through the integration of the nonlinear uniaxial stress-strain response of the individual fibres. The constitutive material laws which characterize the nonlinear behavior of the confined and unconfined concrete and the post-yield strain hardening of the longitudinal steel bars are incorporated in the fiber modeling approach.

The concrete has been demonstrated through a nonlinear confinement concrete model (Figure 6-a), as a good compromise between simplicity and accuracy. For the unstrengthened RC columns confined with transverse steel ties, an uniaxial nonlinear stress-strain relationship and cyclic rules proposed by Mander et al. [40], and the variable confinement algorithm suggested by Madas and Elnashai [41], later modified by the cyclic rules proposed by Martinez-Rueda and Elnashai [42] for numerical stability reasons under large deformations, are used in SeismoStruct program[39]. For the Strengthened RC columns, the confinement effects with FRP wraps are modeled through the employment of the rules proposed by Spoelstra and Monti [43].

The stress-strain behavior of the reinforcing steel (see Figure 6-b) was represented by the nonlinear stress-strain relationship and cyclic rules proposed by Menegotto and pinto [15], and also included additional improvements by Filippou et al. [44] to account for isotopic strain hardening rules [39].

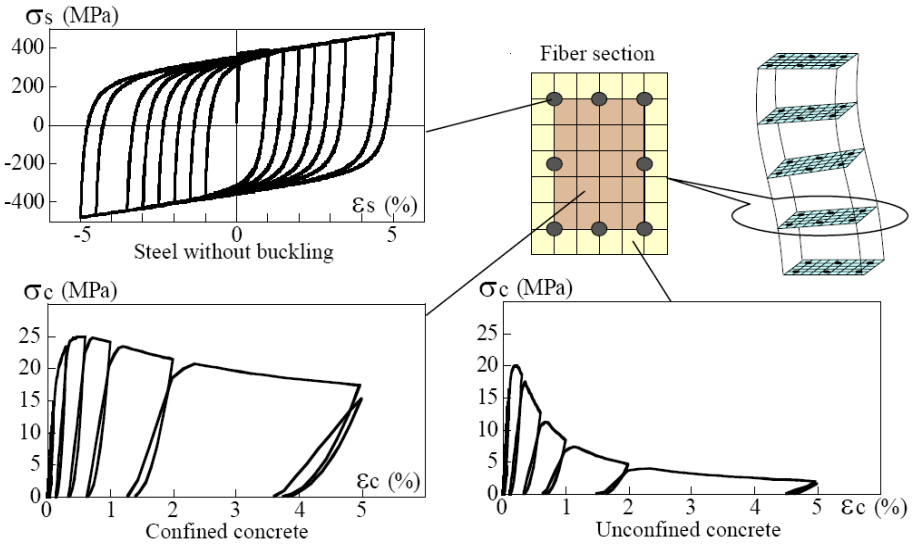

Figure 5. Fiber-based model and constitutive material laws for the nonlinear behavior of confined and unconfined concrete and post-yield strain hardening of steel bar

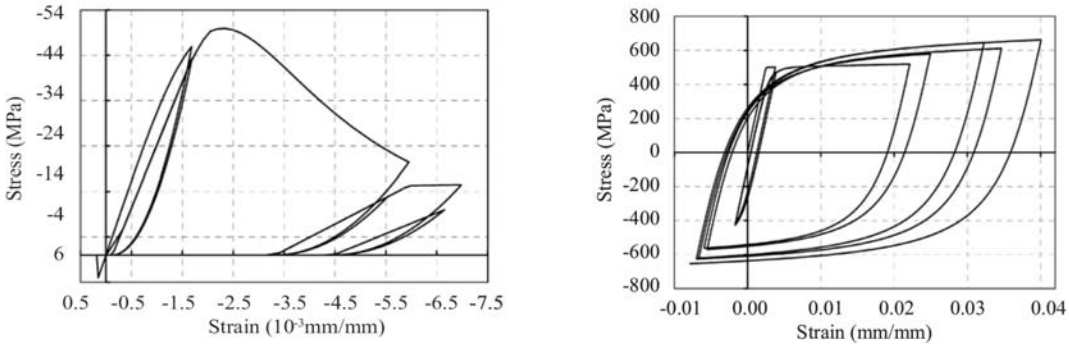

a) b)

Figure 6. Constitutive material laws: a) nonlinear confinement concrete model; b) Menegotto-Pinto steel model with Filippou isotropic hardening

The calibrating parameters in the model, which fully characterize the mechanical properties of concrete and steel, have been defined as shown in Table 3 and 4. Two basic assumptions are made in this study, including plane sections remain plane and perfect bond is assumed between the concrete and longitudinal GFRP bars.

Table 3: Parameters for the Mander et al. nonlinear confinement concrete model, Madas and Elnashai model along with the cyclic rules proposed by Martinez-Rueda and Elnashai

Parameter	**value**
Tensile strength (MPa)	3.5
Strain at unconfined peak stress (mm/mm)	0.002

Table 4: Parameters for the Menegotto-Pinto steel model, with Filippou isotropic hardening

Parameter	**value**
Transition curve initial shape parameter	20
1st transition curve shape coefficient	18.5
2nd transition curve shape coefficient	0.15
1st isotropic hardening coefficient	0.025
2nd isotropic hardening coefficient	2

As illustrated in Figure 7, total lateral displacement measured at the top of each column, Δ, is determined with the summation of deformations due to: a) flexure, $\Delta_{flexure}$; b) longitudinal steel bar slip at column ends, Δ_{slip} ; and c) shear, Δ_{shear} .

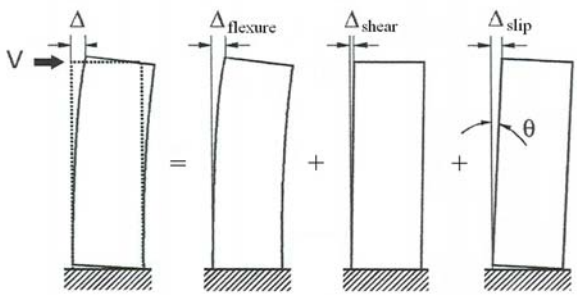

Figure 7. The contribution of displacement components to total lateral displacement

For a typical beam-column member, lateral displacement due to flexure is obtained by integrating the flexural curvatures along the height of the columns.

When a crack at the beam-column interface leads to a large opening, the axial strain may lead to an increase and bond deterioration is concluded between steel and concrete. As a result of bond deterioration and the penetration and accumulation of axial strains along the tensile steel reinforcing bars inside the beam-column joint, the elongation and slip of the longitudinal steel bars at the interface can be considerable. This elongation and slip of tensile reinforcing bars at beam-column interface can result in rigid-body rotation of the column, which is not included in the flexural analysis where the column ends are assumed to be fixed (Figure 8). This additional rotation at beam-column fixed-end can significantly increase the total lateral displacement [45-48]. The bar slip model utilized in this study, have been developed by Sezen and Moehle [47], and includes additional developments by Sezen and Setzler [48]. The slip resulting from accumulated axial strains in the longitudinal steel bar, embedded in the beam-column joint or in the footing, can be determined by integrating the strains over the portion of the bar between the interface and the point with no axial strain. By applying a bilinear strain distribution shown in Figure 8, the slip can be derived from the Equations (1) and (4), [47,48].

$$\begin{aligned} slip &= \int_0^{l_d} \varepsilon \times dx = \left(\varepsilon_s l_d\right)/2 && \varepsilon_s \le \varepsilon_y \\ slip &= \int_0^{l_{dy}} \varepsilon \times dx + \int_{l_{dy}}^{l_{dy}+l'_d} \varepsilon \times dx = \left[\left(\varepsilon_y l_{dy}\right)/2\right] + \left[\left(\varepsilon_s + \varepsilon_y\right) l'_d/2\right] && \varepsilon_s > \varepsilon_y \end{aligned} \tag{1}$$

In this equation, $slip$ is amount of longitudinal steel bar slip at the footing or beam-column interface, l_d is elastic development length, l'_d is development length over the inelastic portion of the reinforcing bar, l_{dy} is development length corresponding to longitudinal steel bar yielding at interface, ε_s is strain in longitudinal steel bar, and ε_y is yield strain. This model assumes a stepped function for bond stress between concrete and steel reinforcements over the embedment length of the bar [49]. The bond stress is taken as, $u_b = 1.0\sqrt{f'_c}\ (MPa)$, for elastic steel strains and a uniform bond stress,

$u'_b = 0.5\sqrt{f'_c}\ (MPa)$, in the portion of the steel reinforcements over which the yield strain is exceeded [49] (Figure 8).

The development lengths over the elastic and inelastic portions of longitudinal steel bar can be derived based on the equilibrium of forces in longitudinal steel bar at the interface, and the stepped function for bond stress from the Equations (2) and (3).

$$l_d = f_s d_b / (4u_b) \tag{2}$$

$$l'_d = (f_s - f_y) d_b / (4u'_b) \tag{3}$$

In these equations, f_s is stress in longitudinal steel bar, f_y is steel yield stress, and d_b is the diameter of longitudinal steel bar. By applying equilibrium at first yielding in longitudinal steel bar and assuming a linear strain distribution along steel reinforcement, by inserting, l_d, and, l'_d, from Equations (2) and (3) into Equation (1), the slip is derived from Equation (4):

$$\begin{aligned} slip &= \left(\varepsilon_s f_s d_b\right) / \left(8\sqrt{f'_c}\right) && \varepsilon_s \le \varepsilon_y \\ slip &= \left[\left(\varepsilon_y f_y d_b\right) / \left(8\sqrt{f'_c}\right)\right] + \left\{\left[(\varepsilon_s + \varepsilon_y)\left(f_s - f_y\right)\right] / \left(4\sqrt{f'_c}\right)\right\} && \varepsilon_s > \varepsilon_y \end{aligned} \tag{4}$$

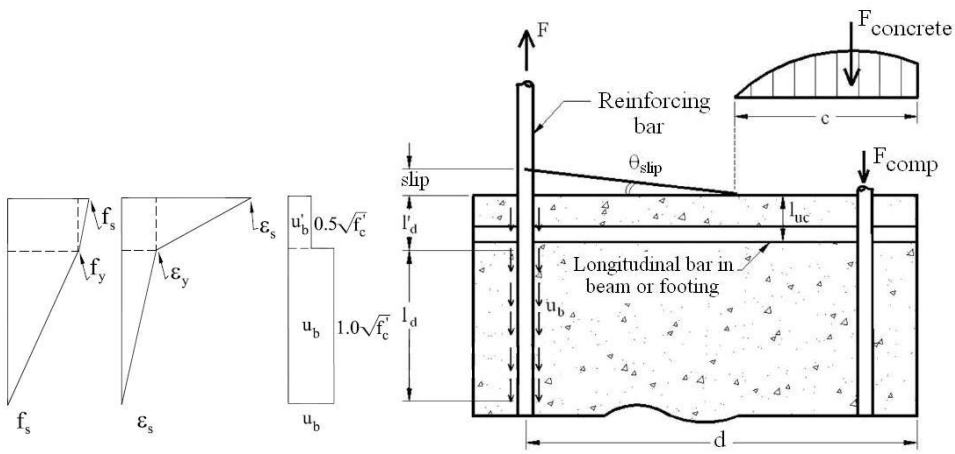

Figure 8. Illustration of bar slip deformation and forces at the beam-column interface

Figure 8 also shows that the section rotation due to the bar slip, θ_{slip}, can be determined by dividing the slip by the width of the open crack, (Equation 5). The width of the open crack is determined from the difference between the section depth, d, and the neutral axis depth, c.

$$\theta_{slip} = slip / (d - c) \tag{5}$$

This rotation is based on the assumption that the section rotates about its neutral axis. Then, substitution of Equation (4) into Equation (5) leads to Equation (6).

$$\begin{aligned} \theta_{slip} &= \left(\varepsilon_s f_s d_b\right) / \left[8\sqrt{f_c'}(d-c)\right] && \varepsilon_s \le \varepsilon_y \\ \theta_{slip} &= \left\{ \left(d_b\right) / \left[8\sqrt{f_c'}(d-c)\right] \right\} \times \left[\varepsilon_y f_y + 2(\varepsilon_s + \varepsilon_y)(f_s - f_y)\right] && \varepsilon_s > \varepsilon_y \end{aligned} \tag{6}$$

As shown in Figure 9, the rotation due to the bar slip can be assumed to be concentrated at the beam-column interface in the form of rigid body rotation.

If the slip-rotation at the top and bottom of a double-curvature column with a length L is known, total lateral displacement due to bar slip can be determined from equation (7).

$$\Delta_{slip} = (\theta_{slip,top} + \theta_{slip,bottom})L \tag{7}$$

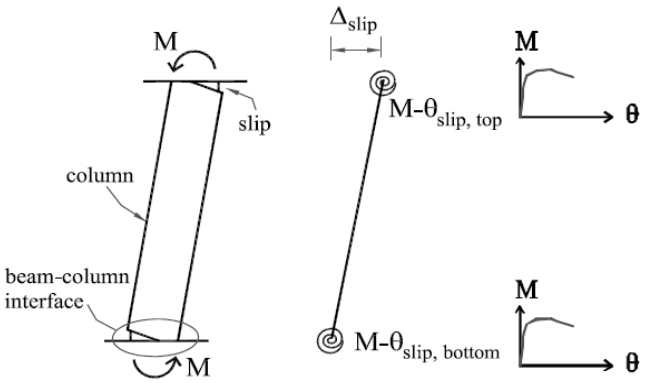

Figure 9. Slip displacement model

Based on the experimental result, the measured shear deformations in the unstregthened and strengthened reference columns have small contribution of 5 to 15 percent of the total lateral displacement. However, the utilized fiber-based modeling software did not enable to simulate shear flexibility; the prediction of the deformation of the reinforced concrete columns was still fairly good. The above mentioned modeling procedure has been utilized to predict the maximum lateral force of the columns under axial and cyclic lateral loads.

2.5 The Comparison of the Numerical Analyses with the Experimental Results

The comparison of the experimental and analytical results is shown in Table 5. The differences between the maximum lateral forces predicted by the fiber-based models, V_{model}, and the measured maximum lateral forces in the experimental results, $V_{\exp}$, revealed that the maximum error is 7%; therefore, the peak lateral forces are nearly equivalent for both the experimental and analytical results.

The maximum lateral forces in numerically reproducing models, V_{model}, are slightly

greater than those of the experimental results, $V_{\exp}$. These numerical overestimations can be explained by the fact that, the fiber-based numerical methodology utilized herein did not feature the possibility of modeling shear flexibility. In this correspondence, it is noted that due to the incidence of the shear damage, the stiffness of these RC columns was not reduced. Nonetheless, the prediction of the maximum lateral forces was still fairly good.

The envelop curves of hysteretic loops for the experimental and analytical unstrengthened reference specimens C_1 and C_2 and strengthened reference specimens R_1 to R_5 are shown in Figure 10 and Figure 11. As shown in the figures, the analytical models represent good agreement with the experimental results.

Table 5: The Comparison of the analytical and experimental results

Specimen	$\frac{P}{f_c' A_g}$	ρ_{NSM} **(%)**	**Maximum lateral force, (kN)**		**Error in maximum lateral force (%)**
			$V_{\exp}$	V_{model}	
C_1	0	na	27	29	7
P_1	0	0.1	-	35	-
P_2	0	0.2	-	40	-
P_3	0	0.3	-	45	-
P_4	0	0.4	-	50	-
R_2	0	0.5	51	52	2
C_2	0.2	na	59	60	2
R_1	0.2	na	62	63	2
R_3	0.1	0.5	64	65	2
P_5	0.2	0.1	-	68	-
P_6	0.2	0.2	-	73	-
P_7	0.2	0.3	-	78	-
P_8	0.2	0.4	-	83	-
R_4	0.2	0.5	84	88	5
R_5	0.2	0.75	101	104	3

Note: $V_{\exp}$, measured maximum lateral force; V_{model}, maximum lateral force predicted by the model; Error in maximum lateral force (%) = 100 × (Analytical – Experimental) / (Experimental); na, not applicable

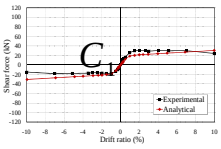

a)

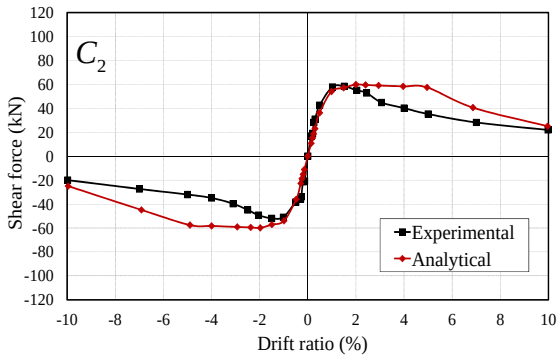

b)

Figure 10. Envelop curves of hysteretic loops for the experimental reference columns and the numerical models: a)C_1; b)C_2

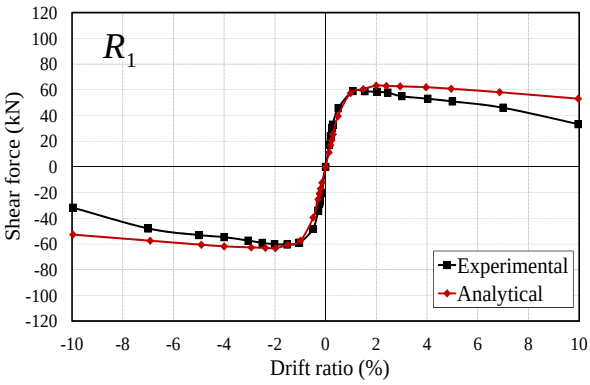

a)

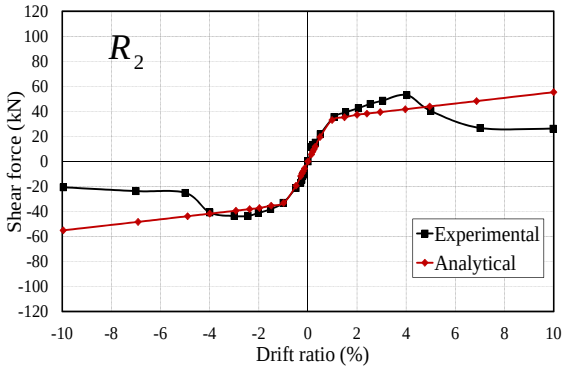

b)

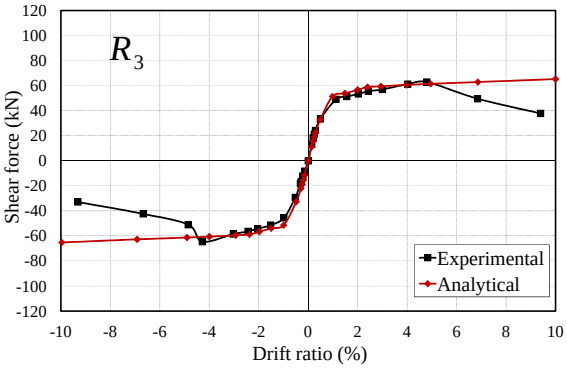

c)

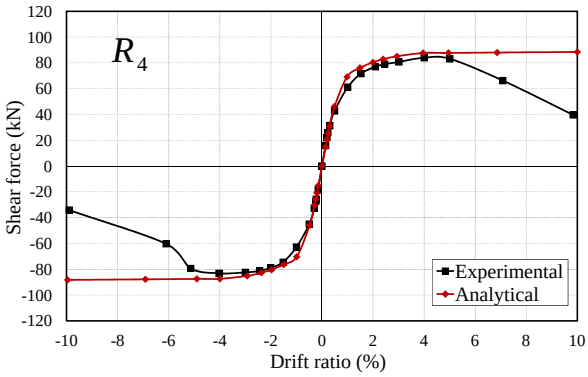

d)

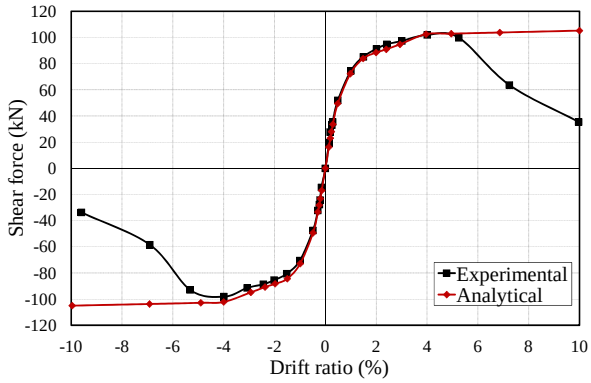

e)

Figure 11. Envelop curves of hysteretic loops for the experimental strengthened reference columns and the numerical models: a) R_1; b) R_2; c) R_3; d) R_4; e) R_5

3. ANALYTICAL RESULTS AND DISCUSSION

The numerical results represent good correlation between fiber-based element modeling approach and the experimental results of the RC columns. Consequently, the numerical models explicitly illustrate a considerable enhancement in the flexural strength of the RC columns retrofitted with Glass Fiber Reinforced Polymer bars.

The simulation of the specimens with fiber-based models shows that, in the strengthened specimens with the axial load level, $P = 0.2 f_c' A_g$, by increasing the GFRP bar reinforcement ratio, ρ_{NSM}, from 0.1% in the column P_5 to 0.75% in the column R_5, the flexural strength of the RC columns is upgraded form 8% to 65%, respectively (see Table 5).